Response of Export Production and Dissolved Oxygen Concentrations to pCO₂ and Temperature Stabilization Scenarios

T. Beaty[1], A. M. E. Winguth[2], and C. Heinze[3,4]

[1]{New Mexico Consortium-Biological Laboratory, Los Alamos, New Mexico}

[2]{Department of Earth and Environmental Sciences, University of Texas at Arlington, Arlington, Texas}

[3]{Geophysical Institute, University of Bergen, and Bjerknes Centre for Climate Research, Bergen, Norway}

[4]{Uni Research Climate, Bergen, Norway}

Correspondence to: T. Beaty (tbeaty@newmexicoconsortium.org)

Abstract

Dissolved oxygen (DO) concentration in the ocean is an important component of marine biogeochemical cycles and will be greatly altered as climate change persists. In this study a global oceanic carbon cycle model (HAMOCC 2.0) is used to address how mechanisms of oxygen minimum zones (OMZ) expansion respond to changes in CO_2 radiative forcing. Atmospheric pCO₂ is increased at a rate of 1% annually and the model is stabilized at 2 X, 4 X, 6 X, and 8 X preindustrial pCO₂ levels. With an increase in CO_2 radiative forcing, the OMZ in the Pacific Ocean is controlled largely by changes in particulate organic carbon (POC) export, resulting in increased remineralization and thus expanding the oxygen minimum zones within the tropical Pacific Ocean. A potential decline in primary producers in the future as a result of environmental stress due to ocean warming and acidification could lead to a substantial reduction of vertical carbon flux and thus increased DO concentration particularly in the Pacific Ocean at a depth of 600-800 m. In contrast, the vertical expansion of the OMZs within the Atlantic and Indian Oceans are linked to reduced oxygen solubility due to rise in potential temperature and to a lesser extent changes in remineralization rates. Changes in oxygen solubility also lead to the formation of a new OMZ in the western sub-

1 tropical Pacific Ocean. The development of the new OMZ results in dissolved oxygen

2 concentration of ≤50 μmols throughout the equatorial Pacific Ocean at 4 times preindustrial

3 pCO_2. Total ocean area with dissolved oxygen concentrations of ≤50 μmols increases by

4 2.5%, 4.5%, and 7.6% for the 2 X, 4X, and 8 X CO_2 simulations, respectively.

5

1   Introduction

7 Rapid increases in concentrations of greenhouse gases (CO_2, CH_4, and N_2O) in the

8 atmosphere since the 18th century have led to greenhouse gas radiative forcing and

9 temperature change of 0.068 °C dec^{-1} (Karl et al. 2015). Atmospheric CO_2 concentrations are

10 predicted to continue to rise from the pre-industrial level of 280 ppmv up to ~800 ppmv by

11 the year 2100 (IPCC 2013) or 2000 ppmv by year 2400 under the assumption that all fossil

12 fuel reservoirs are emitted into the atmosphere (Caldeira and Wickett 2003, Zachos et al.

13 2008). The anthropogenic CO_2 will be partially sequestered by the ocean and by the biosphere

14 on time scales on the order of 10^4 years. An increase in global temperature tends to keep CO_2

15 in the atmosphere due to the decreased solubility of CO_2 in the ocean. In addition, the ocean

16 buffer capacity decreases with rising pCO_2.

17 Changes in climate as a result of CO_2 emission will affect the oxygen distribution in the

18 ocean. DO (dissolved oxygen) concentration in the ocean is affected not only by solubility but

19 also by the biological pump (Volk and Hoffert 1985), which is controlled by export

20 production, vertical carbon flux and decay of particulate organic carbon, and by the transport

21 of biogeochemical tracers by the ocean circulation. Variations in seasonal and long-term DO

22 concentration have been observed in sub-polar and subtropical regions (Whitney et al. 2007,

23 Stramma et al. 2008). Climate models predict that DO concentrations in the ocean will

24 continue to decline with the warming of the deep-sea due to the subsequent decline in

25 solubility as well as variations in the biological pump due to changes in mixing and enhanced

26 ocean stratification. The decrease of the DO concentration will likely result in the expansion

27 of oxygen minimum zones (Sarmiento and Orr 1991, Sarmiento et al. 1998, Schmittner et al.

28 2008, Shaffer et al. 2009) and a significant expansion of bottom water hypoxia (<10 μmol O_2

29 L^{-1}).

30 There are five major non-seasonal OMZs discussed in the current literature, which are the

31 eastern sub-tropical North Pacific OMZ (~15°-25°N), the eastern tropical Pacific OMZ

32 (equatorial region), the eastern South Pacific OMZ (~15°-40°S), the Arabian Sea, the Bay of

1   Bengal (Kamykowski and Zentara 1990, Karstensen et al. 2008, Paulmier et al. 2011), and

2   one low oxygen zone (LOZ) or seasonal OMZ in the equatorial Atlantic. There is limited

3   literature discussing the variability of the Atlantic and Indian Ocean OMZs; however, areas of

4   the eastern North Atlantic OMZ are hypoxic with DO concentrations ranging from 40 to <2

5   μmol kg^{-1} (Stramma et al. 2009, Karstensen et al. 2015). Pacific OMZs have been discussed

6   extensively and there is strong evidence that expansion is already occurring (Oschlies et al.

7   2008, Stramma et al. 2008, Keeling et al. 2010, Stramma et al. 2012). An expansion of the

8   OMZ, a shoaling of the depth of hypoxia (DOH; shallowest depth at which OMZ criteria is

9   met), or a shoaling of the OMZ cores into the photic zone could have severe impacts most

10   notably the decline in ecosystems in the ocean.

11   In this study, the core of the OMZ is defined as a dissolved oxygen concentration of ≤ 20

12   μmol L^{-1} O$_2$ consistent with Helly and Levin 2004, Fuenzalida et al. 2009, and Paulmier et al.

13   2011. The OMZ boundaries are described to have a DO concentration of 50 μmol L^{-1}. The

14   maximum DO concentration of 50 μmol L^{-1} is more stringent than upper limits in other

15   studies (Whitney et al. 2007, Karstensen et al. 2008); however, at these DO concentrations

16   most microorganisms cannot survive (Kamykowski and Zentara 1990, Gray et al. 2002,

17   Sarmiento and Gruber 2006, Paulmier et al. 2011) and therefore considered a reasonable

18   criterion for non-seasonal OMZ. This study focuses on the extent and physical properties of

19   oxygen minimum zones expansion as well as the formation of new OMZs under future

20   emission scenarios including the mechanisms that lead to OMZ intensification.

21

22   **2   Model Description**

23   This study is conducted with the Hamburg Oceanic Carbon Cycle Model Version 2.0

24   (HAMOCC 2.0), which has been expanded to include an iron cycle, sedimentary phosphorus

25   cycle, and improved atmospheric dust parameterization (Palastanga et al. 2011, Palastanga et

26   al. 2013). HAMOCC was originally developed by Maier-Reimer and Hasselmann (1987) and

27   Maier-Reimer (1993). The annually averaged version is computationally very economical and

28   suitable for long-term carbon cycle simulations of several 10,000 years (Maier-Reimer and

29   Hasselmann, 1987, Heinze and Maier-Reimer, 1999). The model utilizes an E-grid (Arakawa

30   and Lamb 1977) and has a horizontal resolution of ~3.5° x 3.5° with grid points 1.25° north

31   and south of the equator to resolve the equatorial upwelling belt. The model contains 11

32   layers (centered at 25,75,150, 250, 450, 700, 1000, 2000, 3000, 4000, and 5000 meters) with a

3

1 total depth of 5000 meters (Heinze et al. 1999, Heinze et al. 2006, Heinze et al., 2009).

2 HAMOCC 2.0 includes a sediment module with porewater and solid components that are

3 coupled by a reaction rate. The sediment module includes one 10 cm thick layer of

4 bioturbated sediment, which is further divided into 11 sub-layers. A more detailed description

5 of the sediment module can be found elsewhere (Heinze et al. 1991, Heinze et al. 1999,

6 Heinze 2004).

7 Transport of tracers is simulated using present-day flow and hydrographic fields (Winguth et

8 al., 1999) from the Hamburg Large-Scale Geostrophic (LSG) model (Maier-Reimer et al.

9 1993). The advection of tracers is iteratively solved by an upstream formulation (Maier-

10 Reimer and Heinze 1993). Atmospheric CO_2 and O_2 are exchanged between the ocean surface

11 (top 50 m) and zonally mixed atmospheric boxes. The air-sea gas exchange of CO_2 is

12 determined by the difference in the partial pressure of CO_2 in the sea surface and the

13 atmospheric pCO_2, the gas transfer velocity, and the requirement for a full equilibration of the

14 surface layer inorganic carbon system. The gas exchange of oxygen is an order of magnitude

15 faster than that of CO_2. Oxygen exchange is carried out according to a fixed transfer velocity

16 and is assumed to be at equilibrium between the atmospheric layer and the surface water at

17 the temperature and salinity-dependent saturation level. The solubility of dissolved oxygen

18 depends on temperature, salinity, and pressure (Weiss 1970). The O_2 flux into the atmosphere

19 is neglected since the atmospheric concentration of O_2 is by far larger than the DO

20 concentration at the ocean surface.

21 The temperature-dependent annual export production of particulate organic carbon (POC) and

22 opal from the euphotic zone is calculated via Michaelis Menten kinetics (Parsons and

23 Takahashi 1973) and $CaCO_3$ production is dependent on the particulate organic and opal

24 production. This relationship is based on the assumption that in the present day ocean there is

25 a dominance of the silicate producers (e.g. diatoms) over the calcareous plankton (e.g.

26 coccolithophores) (Falkowski et al. 2007) . The POC export from the surface into the deep sea

27 is determined from organic carbon production in the uppermost layer and then transported to

28 the deep with a uniform sinking rate of 120 m day^{-1}. Remineralization of organic matter

29 depends on the availability of oxygen for consumption in the water column. Remineralization

30 of POC occurs as long as dissolved O_2 is larger than the minimum O_2 concentration $[O_{2min}]$ =

31 10^{-5} mol L^{-1} for bacterial decomposition of POC. A more detailed description of the model

32 can be found elsewhere (Maier-Reimer and Hasselmann 1987, Heinze et al. 1991, Maier-

1   Reimer and Heinze 1999, Heinze et al. 1999, Palastanga et al. 2011, Palastanga et al. 2013,

2   Beaty-Sykes 2014).

3

4   **3   Experimental Design**

5   The annually averaged version of the model was integrated to quasi-equilibrium state (200

6   kyr) with a stable atmospheric CO_2 concentration of 279.78 ppmv. The reference experiment

7   as well as all sensitivity experiments is started from the near-equilibrium state and integrated

8   for 30,000 yrs. For the reference experiment, the model is forced from preindustrial flow

9   fields of the LSG simulation with a globally averaged potential temperature of 3.78°C and a

10 globally averaged salinity of 34.8 psu (Winguth et al. 1999).

11 Carbon cycle sensitivity experiments are conducted in two sets of scenarios. The first set of

12 scenarios consists of a perturbation of the atmospheric CO_2 concentration relative to

13 preindustrial atmospheric levels pCO_{2ref}; PAL) of 2 X CO_2, 3 X CO_2, 4 X CO_2, 6 X CO_2, and

14 8 X CO_2 to explore the sensitivity of distribution of dissolved oxygen concentration to rising

15 atmospheric pCO_2 level. In these simulations, all other boundary conditions and model

16 parameters are kept at preindustrial levels (Table 1). In a second set of experiments the pCO_2

17 levels are accompanied by the associated changes of temperature at the sea surface as well as

18 in the deep sea to investigate the response of the dissolved oxygen distribution to increases in

19 CO_2 radiative forcing. Stabilization scenarios and brief descriptions are listed in Table 2.

20 In the CO_2 perturbation scenarios atmospheric pCO_2 is increased from preindustrial levels by

21 1% each year (t) until the perturbed atmospheric pCO_2 (pCO_{2pert}) is stabilized at its maximum

22 level (pCO_{2max}) by

23 $$for\ pCO_2 < pCO_{2max}: pCO_{2pert} = pCO_{2ref}(1 + 0.01)^t$$

24 $$and\ for\ pCO_2 \geq pCO_{2max}: pCO_{2pert} = pCO_{2max}. \tag{1}$$

25 The 1% increase of atmospheric CO_2 concentration follows the IPCC (2013) business as usual

26 scenario and is stabilized after 70 years for doubling of preindustrial pCO_2 (see also Winguth

27 et al. 2005) The second set of carbon perturbation scenarios includes the feedback of

28 increasing seawater temperature due to rising atmospheric pCO_2 (Fig. 1). Temperature

29 increases as a function of the 1% increase per time step of atmospheric pCO_2 and is

1   determined using Eq. 2 from Hansen et al., (1988) for the radiative forcing of CO_2 with the

2   addition of a climate model sensitivity of A_t=0.6870.

3   $$\Delta T = A_t \, 6.3 \ln\left(\frac{pCO_2}{pCO_{2_{ref}}}\right) \qquad (2)$$

4   Therefore a doubling of pCO_2 results in a homogeneous increase in temperature of ~3°C,

5   which is consistent with the estimate of Archer (2005) and Hansen et al. (1988). Note that this

6   enhanced sensitivity includes climate feedbacks whereas the direct CO_2 warming for 2 X CO_2

7   is ~1.2°C (Ruddiman 2001, Houghton 2004). The resultant temperature change of the ocean

8   for the doubling of pCO_2 for 2 X CO_2, 4 X CO_2, 6 X CO_2, and 8 X CO_2 is 2.8°C, 5.9°C,

9   8.7°C, and 11.5°C respectively (Fig. 1). Solubility and chemical kinetic equilibrium constants

10 of the carbon cycle are adjusted to the changes in pCO_2 and temperature at each time step in

11 the temperature feedback experiments.

12 In addition to experiments with increased pCO_2 with and without radiative forcing a reduced

13 biology scenario is added in which primary productivity and export (Si, $CaCO_3$, and organic

14 carbon) is set to zero following the approach of Maier-Reimer et al. (1996). The reduced

15 biology scenario is simulated with preindustrial pCO_2 (279 ppmv).

16

17 4   Results

18 4.1   Reference simulation

19 The relevant results of the reference experiment will be briefly discussed in this section.

20 Prescribed temperature and salinity taken from Winguth et al. (1999) are comparable to the

21 observed data from the World Ocean Atlas 2013 (referred hereafter as WOA2013; Locarnini

22 et al. 2013, Zweng et al. 2013) and to the simulations of Maier-Reimer (1993). Simulated

23 seawater temperature and salinity are comparable to the World Ocean Atlas 2013 at 3000 m

24 depth. Due to the slow ventilation of the ocean the WOA2013 data at 3000 m is more

25 representative of preindustrial conditions. Compared to WOA2013, cooler simulated

26 temperatures are projected for the Bering Sea by the LSG, leading to greater O_2 solubility at

27 the surface and therefore higher DO concentration than the corresponding data from

28 WOA2013 (Garcia et al. 2013, Locarnini et al. 2013). This bias may be partially linked to the

29 long-term warming trend over the last decades (IPCC, 2013). Dissolved inorganic carbon

1   (DIC) at the surface is similar to the simulations of Maier-Reimer (1993) and the observations

2   from the WOA2013 (Locarnini et al. 2013) with the exception of the Arctic region in which

3   the reference experiment simulated DIC concentrations at approximately 150 umol kg^{-1} less

4   compared to corresponding values simulated by Maier-Reimer (1993). The decreased

5   simulated DIC in the Arctic region of this preindustrial simulation could be due to the

6   addition of dust fields (Mahowald et al. 2006) and Fe and P cycles (Palastanga et al. 2011,

7   Palastanga et al. 2013). Simulated ocean oxygen concentrations are comparable to Maier-

8   Reimer (1993) and the WOA2013. POC, CaCO$_3$, and opal export and sediment composition

9   are comparable to Maier-Reimer (1993). However, the model does trend toward a slightly

10 higher POC in the tropical latitudes compared to Sarmiento and Gruber (2006) who used the

11 chlorophyll concentration and sea surface temperature based empirical algorithm of Dunne et

12 al. (2005). This bias may be linked to overestimation of export production in HAMOCC 2.0

13 linked to nutrient trapping (Najjar et al. 1992) at the equator. In addition, HAMOCC 2.0

14 simulates a slightly elevated export of CaCO$_3$ and opal export compared to corresponding

15 observed values inferred from CaCO$_3$:POC and opal:POC export ratios (Sarmiento and

16 Gruber 2006).

4.2 Model representation of the oxygen minimum zones in the reference simulation

19 Simulated DO distribution in the reference simulation represents all five major non-seasonal

20 oxygen minimum zones of the Pacific Ocean and Indian Ocean and the seasonal OMZ or low

21 oxygen zone (LOZ; defined as dissolved [O$_2$] < 90 μmol L^{-1}) of the eastern South Atlantic

22 Ocean (Fig. 2). However, due to the course model grid, the eastern subtropical and tropical

23 North Pacific OMZ as well as the OMZs in the Indian Ocean (Arabian Sea and Bay of

24 Bengal) are not resolved individually. The LOZ of the eastern South Atlantic Ocean is

25 simulated in the reference experiment with a OMZ core of ~17-19 μmol L^{-1} O$_2$ and therefore,

26 following the OMZ definition proposed here, the LOZ of the Atlantic Ocean is simulated as a

27 non-seasonal OMZ.

28 The simulation is generally agreeable with the extent and depth of the OMZs, and DO core

29 concentration values of the observations. A model-data bias of the OMZ exist in the North

30 Pacific Ocean resulting in the simulated OMZ reaching too far westward with the western

31 boundary near ~180°W. The OMZ is also simulated too deep with a maximum depth of

32 approximately 2300m. The difference in horizontal extent between the model simulation and

1 observed in the eastern North Pacific OMZ may be attributed to the non-consideration of

2 seasonally variability in the simulation. For the sub-tropical South Atlantic Ocean, the

3 simulated OMZ core is located in a water depth ranging from 300 to 700 meters; which is

4 slightly shallower than the OMZ core in the Indian Ocean. The total ocean area with a DO

5 concentration of ≤20 μmol L^{-1} is approximately 8.6% in the reference simulation.

6 **4.3 Sensitivity of the OMZs and global dissolved oxygen concentrations to**

7 **increased pCO$_2$ without radiative forcing**

8 The increased pCO$_2$ simulations that do not include radiative forcing (temperature increase;

9 Eq. 2) result in small increases of dissolved oxygen at the ocean surface due to the

10 enhancement of primary productivity. The small increase in productivity results in increased

11 DO globally. There are only slight changes in the distributions of DO concentration for these

12 simulations as compared to the simulation that include radiative forcing (Fig. 3). Therefore, in

13 order to discuss future changes in the OMZs the following sections address the expansion of

14 each OMZ and OMZ core as well as the global change at 2 X, 4 X, 6 X, and 8 X CO$_2$

15 simulations that include the temperature feedback.

16 **4.4 Sensitivity of the oxygen minimum zones to CO$_2$ radiative forcing**

17 In each of the scenarios that include radiative forcing, the simulated OMZs expand. The

18 results show the formation of a new OMZ core in the tropical western South Pacific Ocean.

19 There are significant changes in the distributions of DO concentrations in all simulations.

20 4.4.1 Simulated OMZ expansion in the eastern tropical Pacific Ocean in

21 response to CO$_2$ radiative forcing

22 For the 2 X CO$_2$ experiment, the OMZ cores (dissolved O$_2$ concentration ≤20 μmol L^{-1}) of the

23 OMZ in the eastern North Pacific Ocean expands to 65°N compared to the extent to 35°N of

24 corresponding OMZ in the 1 X CO$_2$ scenario. This OMZ merges with that of the eastern

25 South Pacific OMZ at the equator and therefore is considered as a single OMZ, hereafter

26 referred to as the eastern Pacific OMZ. At a depth of 450 m it extends northward around the

27 northern boundary of the North Pacific gyre with dissolved oxygen concentrations of ≤20

28 μmol O$_2$ L^{-1} in the Gulf of Alaska. The southern boundary of the eastern Pacific OMZ is

29 located near the coast of Northern Chile at approximately 30°S at 450 meters depth.

30 Compared to the reference simulation, the OMZ in the 2 X CO$_2$ experiment expands 200 km

1 further to the south. The OMZ western boundary increases by approximately 550 km to

2 150°E. The depth of hypoxia (DOH) is between 150-250 meters. The OMZ has a max depth

3 of 1900 meters, 200 meters deeper than the reference simulation. The OMZ core shoals to 380

4 meters; however, it does not deepen in the 2 X CO_2 simulation. The lowest oxygen

5 concentration in the OMZ core is 17 µmol O_2 L^{-1} in this simulation.

6 The horizontal extent of the OMZ in the 4 X CO_2 scenario is similar to the 2 X CO_2

7 experiment with the addition of all of the North Pacific outside of the North Pacific Gyre

8 having a dissolved oxygen concentration of ≤50 µmol L^{-1} at a depth of 450 meters. The depth

9 of hypoxia shoals vertically to between 75-150 m from the surface in the North Pacific Ocean

10 and remains in a depth range of 150-250 m in the South Pacific Ocean. The maximum depth

11 of the Pacific OMZ increases to 2000 m. For the 4 X CO_2 experiment, the OMZ core extends

12 ~100 km west and deepens by 200 m compared to the 2 X CO_2 simulations. The depth of the

13 OMZ core does not change in the 4 X CO_2 simulations compared to the 2 X CO_2 simulations;

14 however, the minimum dissolved oxygen concentration decreases to 14 µmol L^{-1} (Fig. 4).

15 There is further extension of the OMZ core south to approximately 50°S (central coast of

16 Chile) at 450 m depth in the 8 X CO_2 scenario relative to the 4 X CO_2 experiment. The OMZ

17 core, at a depth of ~2000 meters, does not shoal or deepen in the 6 X and 8 XCO_2 compared

18 to the 4 X CO_2 experiment. In the 8 X CO_2 simulation, the core becomes hypoxic with a

19 minimum dissolved oxygen concentration of ≤8 µmol L^{-1}. The 6 X CO_2 experiment results in

20 a minimum dissolved oxygen concentration of ~12 µmol L^{-1} (Fig. 4).

4.4.2 Simulated OMZ expansion in the eastern tropical South Atlantic Ocean in response to CO_2 radiative forcing

23 The horizontal expansion of the OMZ in the eastern South Atlantic in the 2 X CO_2 simulation

24 remains similar to the reference scenario with a southern boundary at approximately 25°S and

25 extends northward along the west coast of Africa to the southern tip of Morocco to

26 approximately 15°N. The depth of hypoxia shoals from between 250-450 m in the reference

27 experiment to 150-250 m. The maximum depth of OMZ increases by 100 m to 1200 m. In the

28 eastern South Atlantic, the OMZ core in the 2 X CO_2 experiment expands relative to the

29 reference experiment southward by 580 km to approximately 19°S and northward by 110 km

30 (~1° northward propagation). In the 2 X CO_2 experiment, the OMZ core expends vertically; it

31 shoals to 450 m and deepens to 915 m, which is 65 m deeper than the reference simulation.

1   The minimum dissolved O_2 concentration is reduced by 1 μmol L^{-1} relative to the reference

2   experiment to 17 μmol O_2 L^{-1}.

3   Relative to the reference simulation, the 4 X CO_2 simulation results in insignificant horizontal

4   expansion of the OMZ in the latitudinal direction. The most notable area of expansion of the

5   OMZ is in the southwest direction in which the southwestern boundary of the eastern South

6   Atlantic OMZ extends to ~30°S and ~20°W. The maximum depth increases by an additional

7   100 m to a depth of 1300 m. The OMZ core expands symmetrically in east-west direction, by

8   about 100 km, encompassing the Gulf of Guinea. The vertical expansion of the OMZ core is

9   negligible between the 2 X and 4 X CO_2 simulations; however, the strength of the core

10   increases significantly with a minimum dissolved O_2 concentration of 12 μmol L^{-1} (Fig. 4).

11   Horizontal expansion of the eastern South Atlantic OMZ does not occur between the 4 X CO_2

12   simulation and the 6 X or 8 X CO_2 scenarios. In the 6 X CO_2 scenario the horizontal extent of

13   the eastern South Atlantic Ocean at 450 m depth is reduced from the 4 X CO_2 simulation,

14   where as in the 8 X CO_2 simulation the horizontal area expands back to the extent of the 4 X

15   CO_2 simulation. The depth of hypoxia remains between 150-250 m depth for both 6 X and 8

16   X CO_2 experiments. The maximum depth of the OMZ increases to 1500 m in the 8 X CO_2

17   simulation. The OMZ core deepens to 1050 m and shoals from the 6 X and 8 X CO_2 scenarios

18   to 375 m. The minimum dissolved O_2 concentration remains at 12 μmol L^{-1} for both the 6 X

19   and 8 X CO_2 simulations (Fig. 4).

4.4.3 Simulated expansion of the OMZ in the tropical Indian Ocean in response to CO_2 radiative forcing.

22   The expansion of the OMZ in the Indian Ocean is limited at the western boundary by the east

23   coast of Africa and the eastern boundary is constrained by the Indonesian archipelago. The

24   Indian Ocean OMZ includes the poorly resolved Arabian Sea and the Gulf of Bengal, which

25   is limited by the Indian subcontinent. Compared to the reference simulation, the OMZ extends

26   southward to 10°S in the 2 X CO_2 simulation and deepens by 100 m to 1100 m. The OMZ

27   core does not expand horizontally but deepens to 900 meters and shoals by 50m to 225

28   meters. The minimum dissolved oxygen concentration is 10 μmol L^{-1} and remains the lowest

29   concentration for each of the emissions scenario (Fig. 4).

30   In the 4 X, 6 X, and 8 X pCO_2 simulations the horizontal expansion in the Indian Ocean OMZ

31   is insignificant but it deepens to 1300 m, 1400 m, 1700 m, respectively. For the 4 X CO_2

1   experiment the OMZ core expands in the western direction to 45°E and deepens by 100 m to

2   1000 m; however, the upper boundary of the OMZ remains unchanged. In the 8 X CO_2

3   simulation the core expands southward by 650 km to approximately 16°S and shoals to 100 m

4   for both the 6 X and 8 X CO_2 scenarios; however, the lower boundary remains unchanged

5   compared to the 4 X CO_2 experiment. The depth of hypoxia is located between 25 m and 75

6   m in the reference experiment and in all CO_2 emission scenarios.

4.4.4 Simulated OMZ formation in the western tropical Pacific Ocean in response to CO_2 radiative forcing

9   An OMZ core (<20 µmol L^{-1} O_2) is simulated in the western tropical Pacific Ocean (143E,

10 2N) near the Bismarck Sea (Fig. 5). This region is modeled as a low oxygen zone (LOZ) in

11 the reference simulation. For the 4 X CO_2 experiment, the OMZ develops in <2000 yr

12 integration with a minimum dissolved oxygen concentration of 17 µmol L^{-1}. The upper

13 boundary of the OMZ core remains unchanged for all perturbation simulations compared to

14 the reference. However, the OMZ core deepens from 725 m at 3 X CO_2 to 1000 m for the 8 X

15 CO_2 simulation.

4.5 Export of particulate organic carbon and changes in global dissolved O_2 concentration in response to CO_2 radiative forcing

18 Total POC production and export production of POC (P_{POC}) from the euphotic zone into the

19 deep sea increases predominantly near the equatorial Pacific with a rise in seawater

20 temperature in response to CO_2 radiative forcing. P_{POC} in the northern Indian and western

21 tropical Pacific decreases in response to enhanced CO_2 radiative forcing, where as changes in

22 the east Atlantic Ocean are insignificant.

23 Global DO concentration decreases most rapidly during the first 2000 years of integration in

24 each carbon perturbation simulation. The reduction in global dissolved oxygen concentration

25 continues on average 1500 years beyond the year in which the peak pCO_2 emission value is

26 reached. The total ocean area with a dissolved oxygen concentration of <50 µmol L^{-1} expands

27 at approximately 2% per ~3°C increase in seawater temperature which corresponds to a

28 doubling of pCO_2. The total ocean area at which the dissolved O_2 concentration is <50 µmol

29 L^{-1} increases by 7.5% in the 8 X CO_2 simulations (Table 1). The increase of hypoxic area in to

30 the photic zone is insignificant (< 0.3%) due to the air-sea gas exchange. However, an area of

11

1   hypoxia forms in the photic zone of the sub-tropical North Pacific Ocean with a dissolved O_2

2   concentration of less than 12 μmol L^{-1}.

3   **4.6   Sensitivity of dissolved oxygen to reduced biological pump and**

4   **atmospheric oxygen concentration**

5   In order to explore the importance of biological pump (soft tissue pump) to the distribution

6   and concentration of dissolved oxygen globally in the ocean we performed an additional

7   experiment in which all productivity is reduced to zero. This simulation, referred hereafter as

8   the reduced biology scenario, is similar to the "Kill Biology" experiment by Maier-Reimer et

9   al. (1996). In this simulation the atmospheric pCO_2 is set to preindustrial levels, which is in

10   contrast to a simulated exponential increase in atmospheric pCO_2 in response to the

11   diminished export production in the study of Maier-Reimer et al. (1996). Due to the reduced

12   export production, the DIC concentrations increase at the ocean surface by >400 μmol kg^{-1}

13   and by >200 μmol kg^{-1} in the intermediate and deep-water masses at mid-latitudes. This leads

14   to a significant rise in total alkalinity by an average of 550 μeq kg^{-1}. As a result, the pH

15   increases by an average of 0.7 units despite the loss of calcification and $CaCO_3$ burial. Note

16   that weathering rates are kept at preindustrial conditions in all simulations. Dissolved oxygen

17   increases by >300 μmol L^{-1} in the deep-sea and >200 μmol L^{-1} in the intermediate water

18   masses. The dissolved oxygen gradient in this reduced biology scenario is controlled by the

19   air-sea gas exchange of O_2 at the surface and by the temperature-dependent solubility of

20   oxygen: not by the vertical POC flux, which is set by definition to zero to the "killed"

21   productivity. Thus consumption of oxygen by decay of POC is also diminished (Fig. 6). In an

22   additional experiment, the sensitivity of deep-sea dissolved oxygen concentration to changes

23   in atmospheric O_2 concentration is explored by reducing the atmospheric pO_2 by 50%. The

24   decrease in atmospheric pO_2 does not alter the dissolved oxygen concentration significantly

25   compared to the reference experiment.

26

27   **5   Discussion**

28   In this study we investigate the expansion of OMZ as a result of seawater temperature

29   increase in response to CO_2 radiative forcing. It is important to note that changes in ocean

30   stratification due to ocean temperature and density changes are not simulated and held

31   constant at preindustrial conditions. Therefore, the expansion of OMZs in this study are the

1   result of changes in O_2 solubility and temperature-dependent productivity and therefore may

2   be modest due to no consideration of a weakened connection between the OMZ and the ocean

3   surface in the future (Glessmer et al. 2011). It has been suggested that the depth and strength

4   of the thermocline may influence OMZ expansion and contraction (Deutsch et al. 2007). An

5   increase of the thermocline in a warmer climate may result in a contraction of the OMZs due

6   to reduced oxidative demand in hypoxic waters. However, this study assumes a constant

7   thermocline depth, as the temperature increase is uniform at all depths. Other assumptions in

8   this study are a constant nutrient inventory and Redfield ratio. Changes in the elemental

9   stoichiometry (carbon overconsumption) due to rising pCO_2 has been suggested as a possible

10   mechanism of enhanced volume of suboxic water in the ocean due to the respiration of

11   increased organic carbon (Oschlies et al. 2008, Riebesell et al., 2007). Measurements of

12   dissolved oxygen concentration in the suboxic regions of the oceans are limited (Levitus et al.

13   2013, Locarnini et al. 2006); however, paleo-records and climate models support the

14   assumption that ocean anoxic events occur during periods of high pCO_2 (Knoll et al., 1996;

15   Falkowski et al. 2011). Furthermore, OMZs have expanded and contracted during the glacial

16   interglacial cycles (Galbraith et al. 2004) as well as on shorter time scales in response to

17   Dansgaard-Oeschger (D-O) events (Cannariato and Kennett 1999).

18   The simulations of this study agree with other studies of model-simulated change and

19   observed change in the extent of OMZs (Whitney et al. 2007, Karstensen et al. 2008,

20   Stramma et al. 2008, Shaffer et al. 2009, Falkowski et al. 2011). However, the simulations

21   presented here have a greater overall decrease in global oxygen concentration of 9.1% after

22   300 years of integration for a doubling of pCO_2 than previous studies, which range from 1-7%

23   for various pCO_2 emissions and integration times (Matear et al. 2000, Bopp et al. 2002,

24   Oschlies et al. 2008, Schmittner et al. 2008, Bopp et al. 2013). The rapid decrease in global

25   dissolved O_2 concentration is due to the rapid change in global ocean temperature linked to

26   the 1% business as usual atmospheric CO_2 emissions. However, the dissolved oxygen

27   concentrations in the OMZ areas decrease more slowly in the model simulations as compared

28   to the observed trends from Stramma et al., (2008). The study of Stramma et al., (2008)

29   suggests a temperature increase of 0.005 °C yr^{-1} in the Atlantic and Indian Oceans and a

30   temperature decrease by 0.005 C yr^{-1} for the Pacific Ocean since the 1960s. Most of the

31   expansion of suboxic area in this model study occurs during the first 2000 years of the

32   30,000-year simulation due to the slow response time, particularly in the deep Pacific Ocean.

1   The atmospheric pCO_2 is stabilized at the elevated CO_2 concentrations in the carbon

2   perturbation simulations in this study; therefore, no recovery is simulated.

3   In all carbon perturbation simulations the upper boundary of the OMZ cores are

4   shallower compared to the reference simulation. The shallowest OMZ core is found in the

5   Indian Ocean OMZ at ~75 meters. Note that the upper boundary of the OMZ is located at 75

6   m depth because above this depth water masses are influenced by the air sea gas exchange of

7   the uppermost model layer. The core is not expected to shoal beyond 50 m depth in the

8   simulations due to the assumption that the ocean surface oxygen concentration is at

9   equilibrium with the atmosphere and the simulated surface layer of the top 50 meters. The

10   OMZ core of the North Pacific Ocean has the deepest upper boundary, shoaling

11   approximately 100 meters for the highest pCO_2 carbon perturbation scenario. The slower

12   shoaling of the OMZ in the tropical Pacific Ocean compared to that of the tropical eastern

13   Atlantic and Indian Ocean OMZs may be related to difference in solubility as well as linked

14   to a stronger upwelling in the tropical eastern Pacific Ocean. Downward expansion of the

15   OMZ core is limited by the lower boundary of the activity-ventilated zone at approximately

16   2000 meters in the Pacific Ocean. This depth coincides with the depth of the wind-driven

17   circulation, which remains unchanged in each simulation, because the same wind stress

18   forcing is applied to all simulations. Deepening of the eastern South Atlantic OMZ and the

19   Indian Ocean OMZ are also limited to the bottom boundary of the well-ventilated mixed layer

20   (~1500 meter for the Atlantic and ~1000 meters for the Arabian Sea). The ventilation depth of

21   the Arabian Sea may be overestimated in the model due to the lack of monsoon variation,

22   which can cause the mixed layer depth to vary greatly in the Arabian Sea.

23   The expansion of the OMZ in the Indian Ocean and eastern South Atlantic Ocean are

24   controlled primarily by changes in temperature-dependent oxygen solubility and to a lesser

25   extent changes in the temperature-dependent export production of POC. The extent of the

26   OMZ in the Indian Ocean appears to be insensitive to changes in the export of organic matter

27   in response to radiative forcing of less than 6 times of the preindustrial pCO_2. Figure 7

28   displays the increase in outgassing of oxygen at higher pCO_2 levels throughout the tropical

29   regions. The water masses of the present day Arabian Sea and Bay of Bengal are much lower

30   in sea surface dissolved oxygen than either the tropical Atlantic or tropical Pacific OMZs and

31   exhibits a shallower depth of hypoxia. Therefore, any further loss of solubility due to ocean

32   warming would cause an intensification of the OMZ. Findings from this sensitivity study

1 suggest that the expansion of the Indian Ocean OMZ is controlled by solubility changes rather

2 than changes in the export production of POC. The extent of the OMZ in the eastern tropical

3 South Atlantic intensifies mainly due to the change in solubility and exhibits the greatest

4 change in sea surface dissolved oxygen concentration due to CO_2 forcing of all the OMZs

5 simulated. There is an insignificant change in export production of POC in the eastern tropical

6 South Atlantic OMZ. The extent of the present day OMZ has a much higher dissolved oxygen

7 concentration due to cooler water masses than in the northern Indian Ocean. However, the

8 higher salinity of the Atlantic leads to greater loss of O_2 solubility at higher sea surface

9 temperatures as compared to the Indian Ocean or eastern tropical Pacific Ocean for each

10 pCO_2 simulation.

11 The change in the extent of the OMZ in the Pacific Ocean is driven by the change in

12 productivity and export production of POC and increases in remineralization (Fig. 7) and to a

13 lesser degree by changes in temperature-dependent dissolved O_2 solubility. Loss of solubility

14 is greater in the eastern South Atlantic; however, the increase of export production of POC in

15 the eastern equatorial Pacific OMZ leads to significant horizontal expansion, which is not

16 simulated in the eastern South Atlantic. The model does not indicate a more significant

17 increase in export production of POC in the cold tongue of the Pacific Ocean as compared to

18 the warm pool in the western Pacific Ocean. However, it is important to note that the

19 simulated CO_2-induced seawater temperature change is uniform and therefore the eastern

20 Pacific seawater temperature remains cooler relative to other regions of the Pacific Ocean.

21 The Pacific Ocean OMZ does not shoal as significantly as the Indian Ocean or eastern South

22 Atlantic OMZs but expands horizontally under the area of high productivity. Oxygen loss due

23 to remineralization of organic matter is potentially the main mechanism for expansion of the

24 OMZ in the tropical Pacific Ocean. Figure 8 is a cross section of the amount of oxygen

25 consumed by the remineralization of organic matter indicating the large influence of organic

26 matter export in the eastern tropical Pacific OMZ as opposed to eastern South Atlantic OMZ.

27 In the carbon cycle perturbation simulations, the LOZ that currently exists in the western

28 tropical Pacific meets the criteria of a permanent non-seasonal OMZ for the 3 X CO_2

29 simulation; however, in <2000 yrs a much stronger OMZ core develops in the 4 X CO_2

30 simulation. The formation occurs northwest of the Gulf of Carpentaria and expands into the

31 Banda Sea and south along the west coast of Australia. The western tropical Pacific OMZ

32 forms in the warm water masses of the Indonesian throughflow (ITF), which brings warm

1   water westward from the Pacific into the Indian Ocean. The OMZ is then expanded by the

2   oxygen-depleted water masses originating from the Leeuwin Current, which flows south

3   around the west coast of Australia. The controlling mechanism of the formation of the new

4   OMZ core is similar to that of the Indian Ocean OMZ expansion. There is a net loss of export

5   production of POC in the area suggesting the main control of OMZ core formation is loss of

6   O_2 solubility due to increased sea surface temperature (SST) in an area of high heat transport

7   between the Pacific and Indian Oceans. The formation of an OMZ could be expected in this

8   area of higher SST; however, it is important to note that the model does not include changes

9   in the intense tidal induced mixing that may affect sea surface temperatures and dissolved

10   oxygen concentrations within the Indonesian throughflow.

11

12   **6   Conclusions**

13   Increased sea surface temperature as a result of CO_2 radiative forcing will likely cause

14   expansion of present-day tropical OMZs as well as the possibility of the formation of new

15   oxygen depleted regions. Understanding the extent and the mechanisms for these OMZ

16   expansions is of the utmost importance in order to more accurately predict environmental

17   changes in these regions. Simulated expansion of the oxygen minimum zone is greatest in the

18   eastern tropical Pacific Ocean, which is more sensitivity to the change in export of particulate

19   organic carbon and less sensitive to loss of surface oxygen solubility. Total production

20   increases most in the equatorial Pacific leading to the rapid horizontal expansion of the OMZ

21   core. However, a change in the ecosystem structure could alter the C:N stoichiometry (carbon

22   overconsumption) and therefore the expansion of the OMZ in the eastern equatorial Pacific

23   Ocean could be reduced due to decrease in the export production of POC.

24   A rise in the seawater temperature and high salinity in the Atlantic surface water leads to the

25   greatest loss of dissolved oxygen in the intermediate water masses of any of the OMZs

26   simulated. This loss in solubility causes a greater shoaling and deepening in the eastern

27   tropical South Atlantic OMZ rather than horizontal expansion. The Indian Ocean OMZ is

28   restricted in horizontal expansion; therefore, simulated changes in this OMZ are mostly a

29   vertical expansion of the core, which expands at a similar rate as the eastern tropical South

30   Atlantic OMZ due to loss of oxygen solubility in the region, which is already at very low

31   oxygen concentrations.

1   In conclusion, as sea surface temperature increases as a result of CO_2 emission the OMZs will

2   expand and strengthen as a result of changes in solubility and export of POC. These changes

3   will limit migration and habitat zones resulting in fundamental changes in the marine

4   ecosystem. The loss of dissolved oxygen will also result in changes to the carbon and nitrogen

5   cycles. Any expansion of hypoxia into the photic zone could be detrimental to marine

6   ecosystems. Further research on the expansion of OMZ should include changes in ocean

7   circulation and increased stratification in a comprehensive earth system model (see e.g.

8   Moore et al. 2013). Changes in the ventilation of the ocean waters could lead to changes in

9   both the intensity of the oxygen minimum zones as well as any future expansion.

10

11   **Acknowledgements**

17

Biogeosciences
Discussions

Open Access

EGU

1   References

2   Arakawa, A. and Lamb, V.: Computational design of the basic dynamical processes of the UCLA

3   General Circulation Model, Methods in Computational Physics, 17, 174-267, 1977.

4   Archer, D.: Fate of fossil fuel CO_2 in geologic time, Journal of Geophysical Research: Oceans (1978–

5   2012), 110, 2005.

6   Archer, D., Eby, M., Brovkin, V., Ridgwell, A., Cao, L., Mikolajewicz, U., Caldeira, K., Matsumoto,

7   K., Munhoven, G. and Montenegro, A.: Atmospheric lifetime of fossil fuel carbon dioxide, Annu.

8   Rev. Earth Planet. Sci., 37, 117, 2009.

9   Beaty-Sykes, T. M.:, Effects of climate change and perturbation in biogeochemical cycles on oxygen

10   distribution and ocean acidification, PhD Dissertation, University of Texas, Arlington, 2014.

11   Bopp, L., Le Quéré, C., Heimann, M., Manning, A. C. and Monfray, P.: Climate-induced oceanic

12   oxygen fluxes: Implications for the contemporary carbon budget, Global Biogeochem. Cycles, 16,

13   1022, 2002.

14   Bopp, L., Resplandy, L., Orr, J. C., Doney, S. C., Dunne, J. P., Gehlen, M., Halloran, P., Heinze, C.,

15   Ilyina, T. and Séféerian, R.: Multiple stressors of ocean ecosystems in the 21st century: projections

16   with CMIP5 models., Biogeosciences Discussions, 10, 2013.

17   Caldeira, K. and Wickett, M. E.: Oceanography: anthropogenic carbon and ocean pH, Nature, 425,

18   365-365, 2003.

19   Cannariato, K. G. and Kennett, J. P.: Climatically related millennial-scale fluctuations in strength of

20   California margin oxygen-minimum zone during the past 60 ky, Geology, 27, 975-978, 1999.

21   Deutsch, C., Sarmiento, J. L., Sigman, D. M., Gruber, N. and Dunne, J. P.: Spatial coupling of

22   nitrogen inputs and losses in the ocean, Nature, 445, 163-167, 2007.

23   Dunne, J. P., Armstrong, R. A., Gnanadesikan, A. and Sarmiento, J. L.: Empirical and mechanistic

24   models for the particle export ratio, Global Biogeochem. Cycles, 19, 2005.

25   Falkowski, P. G., Knoll, A. H., Falkowski, P. and Knoll, A.: An introduction to primary producers in

26   the sea: who they are, what they do, and when they evolved, Evolution of Primary Producers in the

27   Sea, 1-6, 2007.

1 Falkowski, P., Algeo, T., Codispoti, L., Deutsch, C., Emerson, S., Hales, B., Huey, R., LyONS, T.,

2 NELSON, N. and SCHOFIELD, O.: Ocean De oxygen ation: Past, Present, and Future, Eos, 92, 2011.

3 Fuenzalida, R., Schneider, W., Garcés-Vargas, J., Bravo, L. and Lange, C.: Vertical and horizontal

4 extension of the oxygen minimum zone in the eastern South Pacific Ocean, Deep Sea Research Part II:

5 Topical Studies in Oceanography, 56, 992-1003, 2009.

6 Galbraith, E. D., Kienast, M., Pedersen, T. F. and Calvert, S. E.: Glacial-interglacial modulation of the

7 marine nitrogen cycle by high-latitude O2 supply to the global thermocline, Paleoceanography, 19,

8 2004.

9 Garcia, H. E., Boyer, T. P., Locarnini, R. A., Antonov, J. I., Mishonov, A. V., Baranova, O. K.,

10 Zweng, M. M., Reagan, J. R., Johnson, D. R. and Levitus, S.: World Ocean Atlas 2013: Dissolved

11 Oxygen, Apparent Oxygen Utilization, and Oxygen Saturation, 2013.

12 Glessmer, M., Park, W. and Oschlies, A.: Simulated reduction in upwelling of tropical oxygen

13 minimum waters in a warmer climate, Environmental Research Letters, 6, 045001, 2011.

14 Gray, J. S., Wu, R. S. and Or, Y. Y.: Effects of hypoxia and organic enrichment on the coastal marine

15 environment, Mar. Ecol. Prog. Ser., 238, 249-279, 2002.

16 Hansen, J., Fung, I., Lacis, A., Rind, D., Lebedeff, S., Ruedy, R., Russell, G. and Stone, P.: Global

17 climate changes as forecast by Goddard Institute for Space Studies three-dimensional model, Journal

18 of Geophysical Research: Atmospheres (1984–2012), 93, 9341-9364, 1988.

19 Heinze, C.: Simulating oceanic CaCO3 export production in the greenhouse, Geophys. Res. Lett., 31,

20 2004.

21 Heinze, C., Kriest, I., and Maier-Reimer, E.: Age offsets among different biogenic and lithogenic

22 components of sediment cores revealed by numerical modeling, Paleoceanography, 24.4, 2009.

23 Doi:10.1029/2008PA001662

24 Heinze, C., Gehlen, M. and Land, C.: On the potential of 230Th, 231Pa, and 10Be for marine rain

25 ratio determinations: A modeling study, Global Biogeochem. Cycles, 20, 2006.

26 Heinze, C. and Maier-Reimer, E.: The hamburg oceanic carbon cycle circulation model version

27 "HAMOCC2s" for long time integrations, DKRZ, 1999.

1 Heinze, C., Maier-Reimer, E., Winguth, A. M. and Archer, D.: A global oceanic sediment model for

2 long-term climate studies, Global Biogeochem. Cycles, 13, 221-250, 1999.

3 Heinze, C., Maier-Reimer, E. and Winn, K.: Glacial pCO2 reduction by the world ocean: Experiments

4 with the Hamburg carbon cycle model, Paleoceanography, 6, 395-430, 1991.

5 Helly, J. J. and Levin, L. A.: Global distribution of naturally occurring marine hypoxia on continental

6 margins, Deep Sea Research Part I: Oceanographic Research Papers, 51, 1159-1168, 2004.

7 IPCC 2013.: The IPCC Fifth Assessment Report (AR5), Climate Change 2013: The Physical Science

8 Basis. Intergovernmental Panel on Climate Change, Geneva, Switzerland, 2014.

9 John Theodore Houghton: Global Warming, Cambridge University Press, 2004.

10 Kamykowski, D. and Zentara, S.: Hypoxia in the world ocean as recorded in the historical data set,

11 Deep Sea Research Part A.Oceanographic Research Papers, 37, 1861-1874, 1990.

12 Karl, T. R., Arguez, A., Huang, B., Lawrimore, J. H., McMahon, J. R., Menne, M. J., Peterson, T. C.,

13 Vose, R. S. and Zhang, H. M.: CLIMATE CHANGE. Possible artifacts of data biases in the recent

14 global surface warming hiatus, Science, 348, 1469-1472, 10.1126/science.aaa5632 [doi], 2015.

15 Karstensen, J., Fiedler, B., Schütte F., Brandt, P., Körtzinger, A., Fischer, G., Zantopp, R., Hahn, J.,

16 Visbeck, M., and Wallace, D.: Open ocean dead zones in the tropical North Atlantic Ocean,

17 Biogeosciences Discussions, 11(12), 17391-17411, 2014.

18 Karstensen, J., Stramma, L. and Visbeck, M.: Oxygen minimum zones in the eastern tropical Atlantic

19 and Pacific oceans, Prog. Oceanogr., 77, 331-350, 2008.

20 Keeling, R. F., Körtzinger, A. and Gruber, N.: Ocean deoxygenation in a warming world, Annual

21 Review of Marine Science, 2, 199-229, 2010.

22 Levitus, S., Antonov, J., Baranova, O., Boyer, T., Coleman, C., Garcia, H., Grodsky, A., Johnson, D.,

23 Locarnini, R. and Mishonov, A.: The World Ocean Database, Data Science Journal, 12, WDS229-

24 WDS234, 2013.

25 Locarnini, R., Mishonov, A., Antonov, J., Boyer, T., Garcia, H., Baranova, O., Zweng, M., Paver, C.,

26 Reagan, J. and Johnson, D.: World Ocean Atlas 2013. Vol. 1: Temperature, A.Mishonov, Technical

27 Ed.NOAA Atlas NESDIS, 73, 40, 2013.

1 Mahowald, N. M., Muhs, D. R., Levis, S., Rasch, P. J., Yoshioka, M., Zender, C. S. and Luo, C.:

2 Change in atmospheric mineral aerosols in response to climate: Last glacial period, preindustrial,

3 modern, and doubled carbon dioxide climates, Journal of Geophysical Research, 111, D10202, 2006.

4 Maier-Reimer, E.: Geochemical cycles in an ocean general circulation model. Preindustrial tracer

5 distributions, Global Biogeochem. Cycles, 7, 645-677, 1993.

6 Maier-Reimer, E. and Heinze, C.: , The Hamburg oceanic carbon cycle circulation model.Cycle 1,

7 1992.

8 Maier-Reimer, E. and Hasselmann, K.: Transport and storage of CO2 in the ocean——an inorganic

9 ocean-circulation carbon cycle model, Clim. Dyn., 2, 63-90, 1987.

10 Maier-Reimer, E., Mikolajewicz, U. and Hasselmann, K.: Mean circulation of the Hamburg LSG

11 OGCM and its sensitivity to the thermohaline surface forcing, J. Phys. Oceanogr., 23, 731-757, 1993.

12 Maier-Reimer, E., Mikolajewicz, U. and Winguth, A.: Future ocean uptake of CO2: interaction

13 between ocean circulation and biology, Clim. Dyn., 12, 711-722, 1996.

14 Matear, R., Hirst, A. and McNeil, B.: Changes in dissolved oxygen in the Southern Ocean with

15 climate change, Geochem. Geophys. Geosyst., 1, 2000.

16 Moore, J. K., Lindsay, K., Doney, S. C., Long, M. C. and Misumi, K.: Marine Ecosystem Dynamics

17 and Biogeochemical Cycling in the Community Earth System Model [CESM1 (BGC)]: Comparison of

18 the 1990s with the 2090s under the RCP4. 5 and RCP8. 5 Scenarios., J. Clim., 26, 2013.

19 Najjar, R. G., Sarmiento, J. L. and Toggweiler, J.: Downward transport and fate of organic matter in

20 the ocean: Simulations with a general circulation model, Global Biogeochem. Cycles, 6, 45-76, 1992.

21 Oschlies, A., Schulz, K. G., Riebesell, U. and Schmittner, A.: Simulated 21st century's increase in

22 oceanic suboxia by CO2-enhanced biotic carbon export, Global Biogeochem. Cycles, 22, 2008.

23 Palastanga, V., Slomp, C. and Heinze, C.: Glacial-interglacial variability in ocean oxygen and

24 phosphorus in a global biogeochemical model, Biogeosciences, 10, 945-958, 2013.

25 Palastanga, V., Slomp, C. and Heinze, C.: Long-term controls on ocean phosphorus and oxygen in a

26 global biogeochemical model, Global Biogeochem. Cycles, 25, 2011.

Biogeosciences
Discussions

Open Access

EGU

1 Parsons, T. and Takahashi, M.: Environmental control of phytoplankton cell size, Limnol. Oceanogr.,

2 18, 511-515, 1973.

3 Paulmier, A., Ruiz-Pino, D. and Garçon, V.: CO2 maximum in the oxygen minimum zone (OMZ),

4 Biogeosciences, 8, 239-252, 2011.

5 Riebesell, U., Schulz, K. G., Bellerby, R. G. J., Botros, M., Fritsche, P., Meyerhöfer, M., Neill, C.,

6 Nondal, G., Oschlies, A., Wohlers, J., and Zöllner, E.: Enhanced biological carbon consumption in a

7 high CO2 ocean, Nature, 450(7169), 545-548, 2007. doi:10.1038/nature06267

8 Ruddiman, W. F.: Earth's Climate: past and future, Macmillan, 2001.

9 Sarmiento, J. L., Hughes, T. M., Stouffer, R. J. and Manabe, S.: Simulated response of the ocean

10 carbon cycle to anthropogenic climate warming, Nature, 393, 245-249, 1998.

11 Sarmiento, J. L. and Orr, J. C.: Three-dimensional simulations of the impact of Southern Ocean

12 nutrient depletion on atmospheric CO2 and ocean chemistry, Limnol. Oceanogr., 36, 1928-1950,

13 1991.

14 Sarmiento, J. L. and Gruber, N.: Ocean biogeochemical dynamics, Princeton University Press

15 Princeton, 2006.

16 Schmittner, A., Oschlies, A., Matthews, H. D. and Galbraith, E. D.: Future changes in climate, ocean

17 circulation, ecosystems, and biogeochemical cycling simulated for a business-as-usual CO2 emission

18 scenario until year 4000 AD, Global Biogeochem. Cycles, 22, GB1013, 2008.

19 Shaffer, G., Olsen, S. M. and Pedersen, J. O. P.: Long-term ocean oxygen depletion in response to

20 carbon dioxide emissions from fossil fuels, Nature Geoscience, 2, 105-109, 2009.

21 Stramma, L., Oschlies, A. and Schmidtko, S.: Anticorrelated observed and modeled trends in

22 dissolved oceanic oxygen over the last 50 years, Biogeosciences Discussions, 9, 4595-4626, 2012.

23 Stramma, L., Visbeck, M., Brandt, P., Tanhua, T., and Wallace, D.: Deoxygenation in the oxygen

24 minimum zone of the eastern tropical North Atlantic, Geophysical Research Letters 36(20), 2009.

25 Stramma, L., Johnson, G. C., Sprintall, J. and Mohrholz, V.: Expanding oxygen-minimum zones in the

26 tropical oceans, Science, 320, 655-658, 2008.

1   Volk, T. and Hoffert, M. I.: Ocean carbon pumps: Analysis of relative strengths and efficiencies in

2   ocean-driven atmospheric CO2 changes, The Carbon Cycle and Atmospheric CO: Natural Variations

3   Archean to Present, 99-110, 1985.

4   Weiss, R.: The solubility of nitrogen, oxygen and argon in water and seawater, in: Deep Sea Research

5   and Oceanographic Abstracts, 1970.

6   Whitney, F. A., Freeland, H. J. and Robert, M.: Persistently declining oxygen levels in the interior

7   waters of the eastern subarctic Pacific, Prog. Oceanogr., 75, 179-199, 2007.

8   Winguth, A., Mikolajewicz, U., Gröger, M., Maier-Reimer, E., Schurgers, G. and Vizcaíno, M.:

9   Centennial-scale interactions between the carbon cycle and anthropogenic climate change using a

10   dynamic Earth system model, Geophys. Res. Lett., 32, 2005.

11   Winguth, A., Archer, D., Duplessy, J., Maier-Reimer, E. and Mikolajewicz, U.: Sensitivity of

12   paleonutrient tracer distributions and deep-sea circulation to glacial boundary conditions,

13   Paleoceanography, 14, 304-323, 1999.

14   Zachos, J. C., Dickens, G. R. and Zeebe, R. E.: An early Cenozoic perspective on greenhouse warming

15   and carbon-cycle dynamics, Nature, 451, 279-283, 2008.

16   Zweng, M., Reagan, J., Antonov, J., Locarnini, R., Mishonov, A., Boyer, T., Garcia, H., Baranova, O.,

17   Johnson, D. and Seidov, D.: World Ocean Atlas 2013. Vol. 2: Salinity, NOAA Atlas NESDIS, 74, 39,

18   2013.

19

1 Table 1. List of initial conditions.

2 Table 2. List of model scenarios.

3 Figure 1. Atmospheric pCO_2 and sea surface temperature increase from the reference run (a) 2

4 X CO_2 (b) 4 X CO_2 (c) 6 X CO_2 (d) 8 X CO_2 for the first 500 years of a 30k year simulation.

5 The red dashed line indicates the preindustrial pCO_2 level.

6 Figure 2. Locations of the OMZ at 450 meters depth simulated by HAMOCC 2.0 (reference

7 experiment) [1] Eastern North Pacific OMZ [2] Eastern South Pacific OMZ [3] Eastern South

8 Atlantic OMZ [4] Indian Ocean.

9 Figure 3. Dissolved O_2 concentration simulated by (a) the 4 X CO_2 experiment without CO_2

10 radiative forcing minus the reference experiment (b) the 4 X CO_2 with CO_2 radiative forcing

11 simulation minus reference experiment.

12 Figure 4. Simulated vertical distribution of dissolved O_2 through the OMZ cores for a)

13 Eastern North Pacific OMZ [110°W, 10°N], b) Eastern South Pacific OMZ [85°W, 10°S], c)

14 Eastern South Atlantic OMZ [5°W, 10°S], and d) Indian Ocean OMZ [Gulf of Bengal; 85°E,

15 7°N] for the 1 X, 4 X and 8 X CO_2 simulations (top). The bottom row are finer scale

16 dissolved oxygen profiles for the OMZ cores e) Eastern North Pacific OMZ, f) Eastern South

17 Pacific OMZ, g) Eastern South Atlantic OMZ, and h) Indian Ocean OMZ for the 1 X, 4 X and

18 8 X CO_2 simulations. Observations are the annual statistical mean for dissolved oxygen from

19 the World Ocean Atlas, 2013 (Garcia et al., 2014). Standard error of the mean; upper ocean:

20 0.54-2.86 µmol L^{-1}, twilight zone: 0.42-2.32 µmol L^{-1}, deep ocean: 0.36-1.98 µmol L^{-1}.

21 Figure 5. Zonal cross-section at 1.25° N of the formation of the western tropical Pacific OMZ

22 for the (a) 2 X, (b) 4 X and (c) 8 X CO_2 simulations. The OMZ core is located between 130°E

23 and 150°E.

24 Figure 6. (a) Dissolved oxygen concentration for the extinction simulations and (b) reference

25 simulation oxygen concentration.

Biogeosciences Open Access
Discussions
EGU

1   Figure 7. (a) Difference in export production of POC between the 8 X CO_2 experiment and

2   reference experiment, (b) dissolved oxygen at 450 m depth for the 8 X CO_2 experiment, (c)

3   difference in air-sea gas exchange between the 8 X CO_2 experiment and the reference

4   experiment, and (d) sea-water temperature at 450 m depth. The numbers indicate the OMZ

5   locations; [1] Eastern tropical North Pacific; 110°W, 10°N. [2] eastern tropical South Pacific;

6   85°W, 10°S. [3] eastern tropical South Atlantic; 5°W, 10°S. [4] Indian Ocean (Gulf of

7   Bengal); 85°E, 7°N.

8   Figure 8. (a) Lost due to remineralization of particulate organic carbon for the reference run

9   [μmol m^{-2}yr^{-1}]. Difference between the loss of oxygen due to remineralization between (b) 2

10 X CO_2 and reference run, (c) 4 X CO_2 and reference run (d) 8 X CO_2 and reference

11 experiment.

12

13

14

1   Table 1. List of initial conditions.

Water Column		Atmosphere	
Parameter	Value (mol L^{-1})	Parameter	Value (ppmv)
sCO_2	$2.25\ E^{-3}$	CO_2	279.78
Alkalinity	2.33 (eq)	O_2	209761
PO_4	$2.54\ E^{-4}$		
O_2	$1.65\ E^{-4}$		
Fe dust	$6.0\ E^{-10}$		

1   Table 2. List of model scenarios.

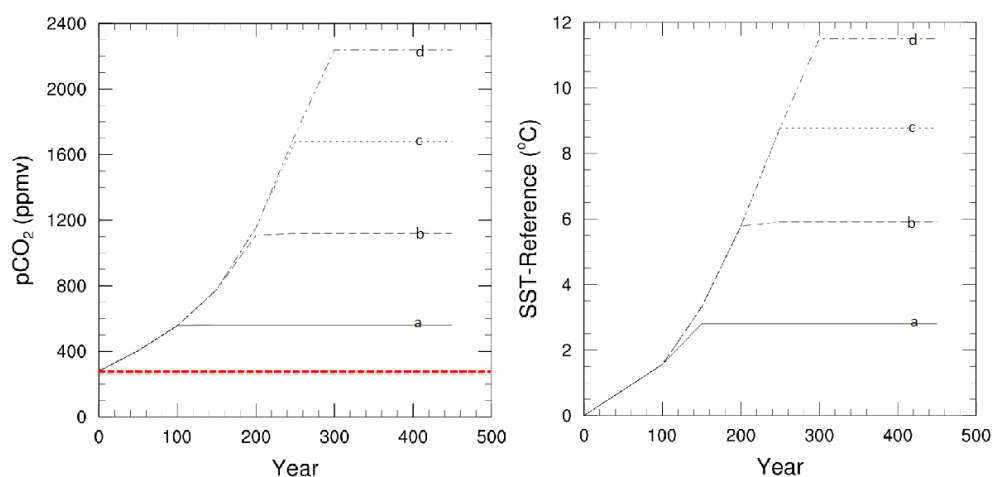| Increased pCO$_2$ without Radative Forcing	Increased pCO$_2$ with Radative Forcing	Atmospheric CO$_2$ Concentration (ppmv)	Total POC Production (PgC yr^{-1})	Integration Time (years)	Brief Description
CO$_2$ Stabilization Experiments					
1 X CO$_2$		279.78	10.53	30,000	Reference simulation with preindustrial atmospheric CO$_2$ levels.
2 X CO$_2$_nf	2 X CO$_2$_f	559.56	10.69	30,000	Experiments with no feedbacks (nf) have an increase of
3 X CO$_2$_nf	3 X CO$_2$_f	839.34	10.72	30,000	pCO$_2$ of 1% per year without temperature feedbacks.
4 X CO$_2$_nf	4 X CO$_2$_f	1,119.12	10.79	30,000	Temperature changes are applied in experiments with feedbacks (f) as a function of pCO$_2$ after Hansen et al.
6 X CO$_2$_nf	6 X CO$_2$_f	1,678.68	10.81	30,000	(1988) resulting in a seawater temperature change of
8 X CO$_2$_nf	8 X CO$_2$_f	2,238.24	10.93	30,000	2.8°C, 5.9°C, 8.7°C, and 11.5°C for 2 X, 4 X, 6 X, and 8 X CO$_2$, respectively.
Reduced Atmospheric Oxygen Concentration and Kill-Biology Experiments					
Kill_atmO$_2$_50		279.78	10.53	1,000	Oxygen solubility simulations include preindustrial pCO$_2$ levels and reduced atmospheric O$_2$ and reduced primary
Kill_all_prod		279.78	10.53	1,000	productivity. Kill_atmO$_2$_50 is simulated with present day productivity and atmospheric O$_2$ reduces by 50%.
Kill_all_prod_50		279.78	10.53	1,000	Kill_all_prod is simulated as an extinction simulation with primary productivity (POC, Si, CaCO$_3$) reduced to 1X10^{-20} PgC yr^{-1} and present day atmospheric O$_2$ concentrations. A final experiment (Kill_all_prod_50) includes the extinction of primary producers (1X10^{-20} PgC yr^{-1}) and a 50% reduction in atmospheric O$_2$.

Figure 1. Atmospheric pCO_2 and sea surface temperature increase from the reference run

(a) 2 X CO_2 (b) 4 X CO_2 (c) 6 X CO_2 (d) 8 X CO_2 for the first 500 years of a 30k year

simulation. The red dashed line indicates the preindustrial pCO_2 level.
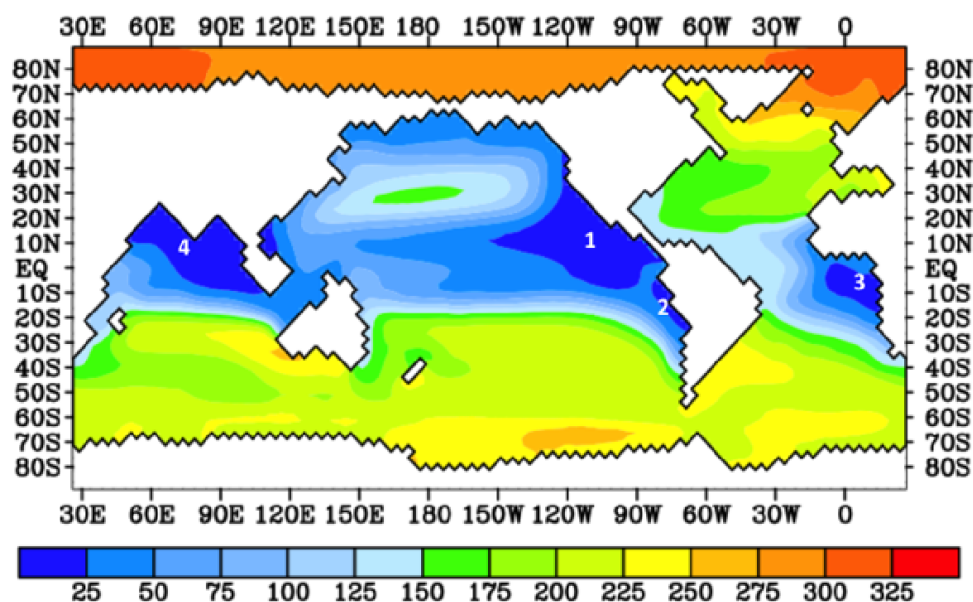
Figure 2. Locations of the OMZ at 450 meters depth simulated by HAMOCC 2.0 (reference experiment) [1] Eastern North Pacific OMZ [2] Eastern South Pacific OMZ [3] Eastern South Atlantic OMZ [4] Indian Ocean.
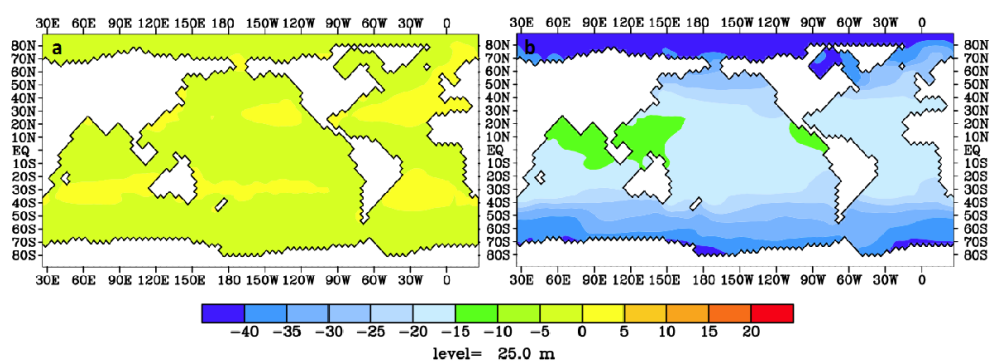

Figure 3. Dissolved O_2 concentration simulated by (a) the 4 X CO_2 experiment without CO_2 radiative forcing minus the reference experiment (b) the 4 X CO_2 with CO_2 radiative forcing simulation minus reference experiment.
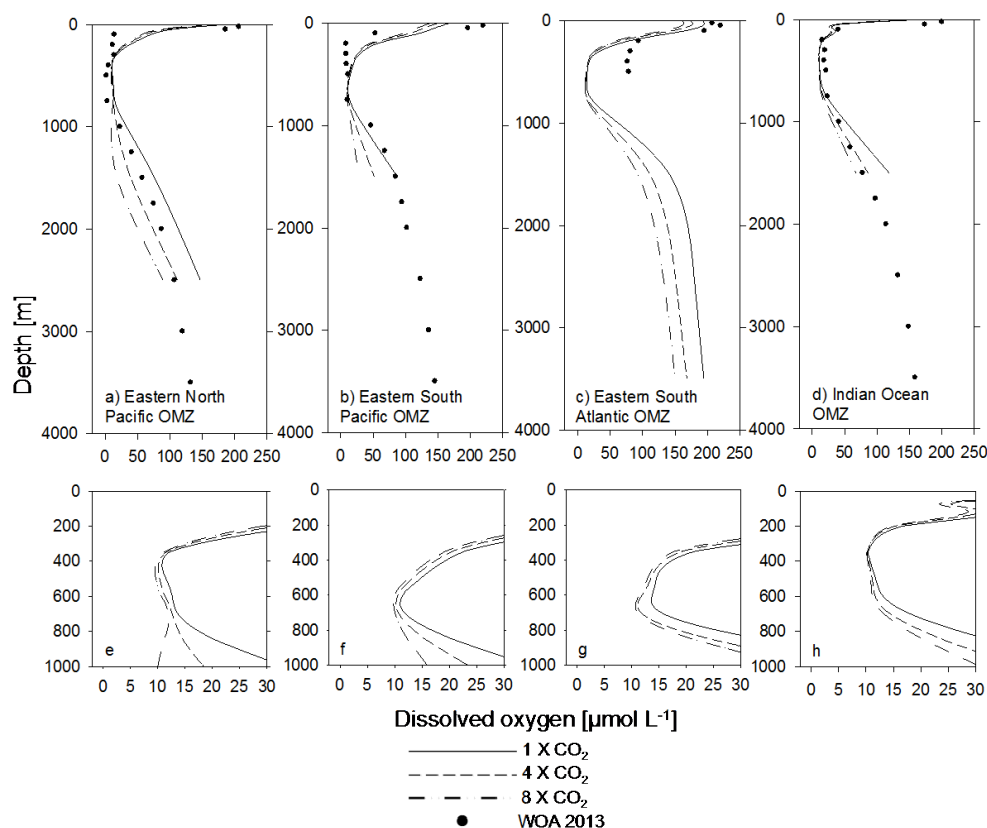
Figure 4. Simulated vertical distribution of dissolved O_2 through the OMZ cores for a) Eastern North Pacific OMZ [110°W, 10°N], b) Eastern South Pacific OMZ [85°W, 10°S], c) Eastern South Atlantic OMZ [5°W, 10°S], and d) Indian Ocean OMZ [Gulf of Bengal; 85°E, 7°N] for the 1 X, 4 X and 8 X CO_2 simulations (top). The bottom row are finer scale dissolved oxygen profiles for the OMZ cores e) Eastern North Pacific OMZ, f) Eastern South Pacific OMZ, g) Eastern South Atlantic OMZ, and h) Indian Ocean OMZ for the 1 X, 4 X and 8 X CO_2 simulations. Observations are the annual statistical mean for dissolved oxygen from the World Ocean Atlas, 2013 (Garcia et al., 2014). Standard error of the mean; upper ocean: 0.54-2.86 μmol L^{-1}, twilight zone: 0.42-2.32 μmol L^{-1}, deep ocean: 0.36-1.98 μmol L^{-1}.

Biogeosciences
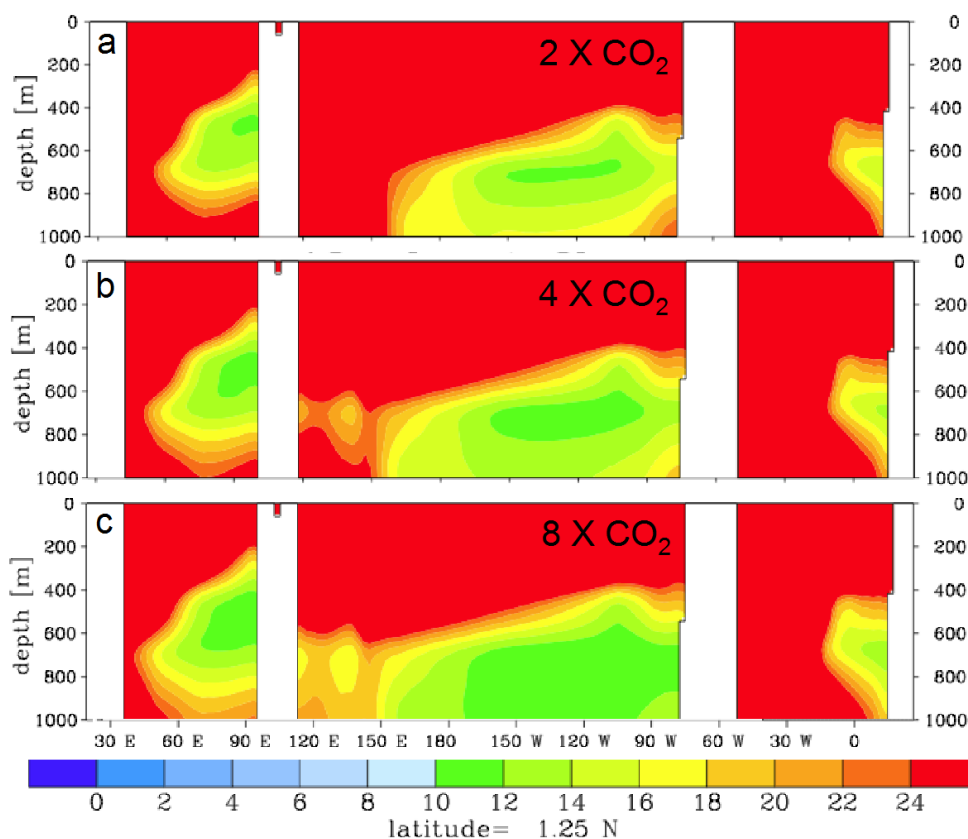Discussions

Open Access

EGU

Figure 5. Zonal cross-section at 1.25° N of the formation of the western tropical Pacific OMZ for the (a) 2 X, (b) 4 X and (c) 8 X CO_2 simulations. The OMZ core is located between 130°E and 150°E.
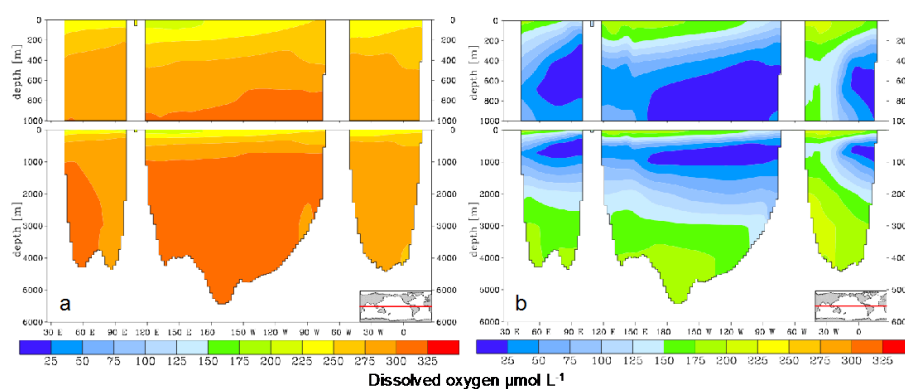
Figure 6. (a) Dissolved oxygen concentration for the extinction simulations and (b) reference simulation oxygen concentration.
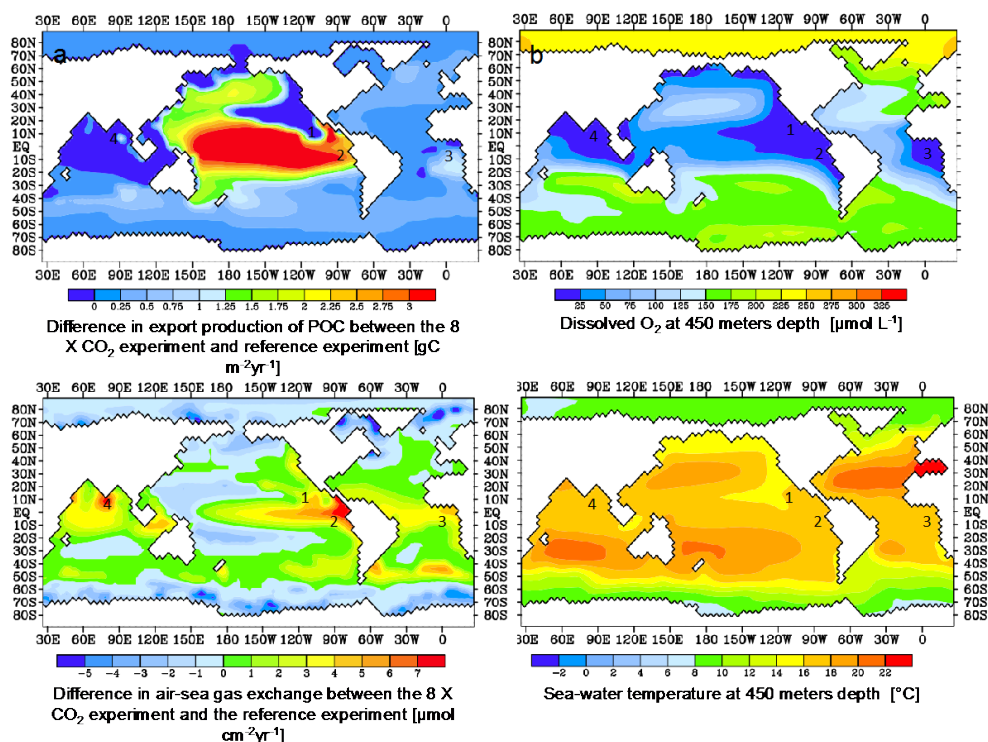
Figure 7. (a) Difference in export production of POC between the 8 X CO_2 experiment and reference experiment, (b) dissolved oxygen at 450 m depth for the 8 X CO_2 experiment, (c) difference in air-sea gas exchange between the 8 X CO_2 experiment and the reference experiment, and (d) sea-water temperature at 450 m depth. The numbers indicate the OMZ locations; [1] Eastern tropical North Pacific; 110°W, 10°N. [2] eastern tropical South Pacific; 85°W, 10°S. [3] eastern tropical South Atlantic; 5°W, 10°S. [4] Indian Ocean (Gulf of Bengal); 85°E, 7°N.
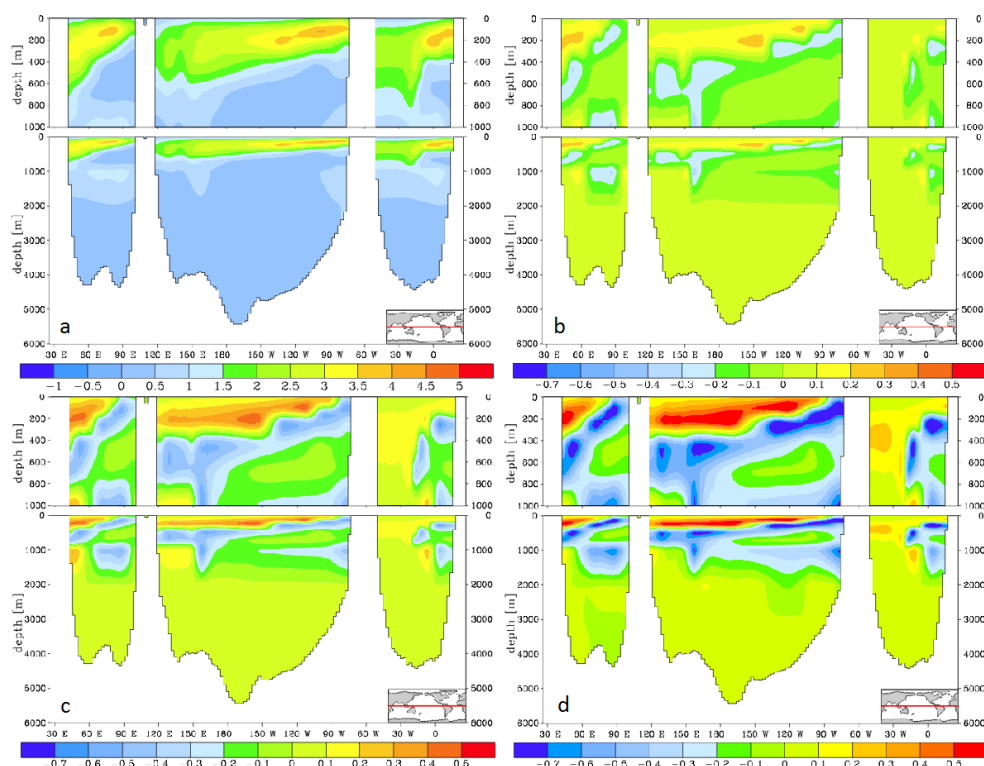
Figure 8. (a) Lost due to remineralization of particulate organic carbon for the reference run [μmol m^{-2}yr^{-1}]. Difference between the loss of oxygen due to remineralization between (b) 2 X CO$_2$ and reference run, (c) 4 X CO$_2$ and reference run (d) 8 X CO$_2$ and reference experiment.